energies

MDPI

Article

Solar-Driven Simultaneous Electrochemical CO_2 Reduction and Water Oxidation Using Perovskite Solar Cells

Jaehoon Chung [1], Nam Joong Jeon [2,*] and Jun Hong Noh [3,*]

[1] Department of Physics and Astronomy, and Wright Center for Photovoltaics Innovation and Commercialization (PVIC), University of Toledo, Toledo, OH 43606, USA; Jaehoon.chung@utoledo.edu
[2] Division of Advanced Materials, Korea Research Institute of Chemical Technology, Daejeon 305-600, Korea
[3] School of Civil, Environmental and Architectural Engineering, Korea University, Seoul 02841, Korea
* Correspondence: njjeon@krict.re.kr (N.J.J.); junhnoh@korea.ac.kr (J.H.N.); Tel.: +82-42-860-7394 (N.J.J.); +82-2-3290-4866 (J.H.N.)

Abstract: The utilization of solar energy into electrochemical reduction systems has received considerable attention. Most of these attempts have been conducted in a single electrolyte without a membrane. Here, we report the system combined by the electrochemical CO_2 reduction on the Au dendrite electrode and the water oxidation on the Co-Pi electrode with a Nafion membrane. An efficient reduction of CO_2 to CO in the cathode using the proton from water oxidation in the anode is conducted using perovskite solar cells under 1 sun condition. The sustainable reaction condition is secured by balancing each reaction rate based on products analysis. Through this system, we collect reduction products such as CO and H_2 and oxidation product, O_2, separately. Employing separation of each electrode system and series-connected perovskite solar cells, we achieve 8% of solar to fuel efficiency with 85% of CO selectivity under 1 sun illumination.

Keywords: solar to fuel; CO_2 reduction; water oxidation; electrochemical; perovskite

Citation: Chung, J.; Jeon, N.J.; Noh, J.H. Solar-Driven Simultaneous Electrochemical CO_2 Reduction and Water Oxidation Using Perovskite Solar Cells. *Energies* **2022**, *15*, 270. https://doi.org/10.3390/en15010270

Academic Editor: Bashir A. Arima

Received: 9 December 2021
Accepted: 28 December 2021
Published: 31 December 2021

1. Introduction

Using solar-driven energy to generate valuable products, such as electricity and chemical products, is a promising strategy to mitigate the dependence on fossil fuels [1]. Among the utilization of solar energy, solar cell technology has achieved remarkable advances in efficiency and stability [2–4]. In addition, artificial photosynthesis is one of the promising candidates paid attention to for solar energy utilization [5]. More recently, many researchers have paid great attention to the collaboration of these two technologies to exploit sunlight, such as water splitting and CO_2 reduction reaction (CO_2RR) using electricity from solar cells [6]. The most common solar-to-fuel technology is solar-to-hydrogen (H_2), splitting the water into H_2 and oxygen (O_2) [7–9]. Although hydrogen is a valuable product to use for the feedstock of fuel cells, solar-to-CO_2RR is the ultimate solution in both alleviating carbon dioxide concentration in our environment and using chemical products as alternative energy sources [10–12]. However, unlike solar-to-H_2, solar-to-CO_2RR demands more challenging criteria, including relatively high reaction potential, product selectivity, and ion exchange between two different electrolytes.

In terms of reaction potential, proper catalyst selection for both reactions (i.e., CO_2RR in the cathode and water oxidation in anode) is necessary to overcome the high barrier of potential solar-to-CO_2RR and water oxidation requirements [13]. Among the various candidates for CO_2RR, gold (Au) is the commonly employed electrocatalyst to minimize the overpotential needed for CO_2 reduction. Au electrocatalyst exhibits the lowest overpotential for CO_2 reduction reaction compared to other metal catalysts such as Ag, Cu, Sn, and Zn [14]. In previous reports, CO_2 reduction with Au nanoparticles was operated from −0.4 to −0.6 V, corresponding to 0.29–0.49 V of overpotential. In addition, Au is well known for the metal electrocatalyst with medium hydrogen overpotential and weak

binding energy toward adsorbed CO (* CO) [15–17]. Due to the thermodynamic advantage of CO_2RR on Au, the product selectivity of CO is superior to the other metal catalysts.

Along with the CO_2 reduction catalyst, water oxidation catalyst in the anode is very important to substantialize solar-to-CO_2RR. Many scientists have reported efficient electrochemical water oxidation catalysts such as Ni-based layered double hydroxide (Ni-LDH), hematite-related compound (Fe_2O_3), RuO_2 and IrO_2 operated with ~0.4 V overpotential in the basic electrolyte [18–21]. However, conventional electrochemical water oxidation catalysts have a significant drawback in their adoption as anodes in the CO_2RR system. According to the reaction mechanism for the water oxidation process in basic media, the anode receives OH^- from the cathode, so it is not suitable for the CO_2RR counterpart [22]. For this reason, water oxidation electrocatalysts operating at neutral media that can supply protons by ion diffusion are recommended for the anode of the solar-to-CO_2RR system. Among the candidate, Cobalt-phosphate (Co-Pi) electrocatalyst for water oxidation is a suitable candidate for anode material that can donate protons by water oxidation with low overpotential (i.e., 0.3 V) in neutral anolyte.

Moreover, to overcome the high potential requirement, it is necessary to adopt solar cells compatible with the solar-to-CO_2RR system. Theoretically, CO_2RR with water oxidation requires at least 1.34 V (vs. RHE); the potential for CO_2 into CO is −0.11 V, and the potential for water oxidation is +1.23 V [10]. In terms of voltage requirement, conventional solar cells, such as Silicon (Si), $CuInGaSe_2$(CIGS), which show 0.7 to 0.8 V of open-circuit voltage(V_{OC}), hardly qualify the high voltage requirement. Perovskite solar cells (PSCs) are attracting significant attention as future solar cells because they can be highly efficient even in low-temperature solution processes. In particular, PSCs are suitable for solar-to-CO_2RR due to their low voltage loss and facile bandgap tunability [23–25]. PSCs have been successfully used in various optoelectronic devices, including solution-processed solar cells with power conversion efficiency (PCE) exceeding 25.5% [26–28]. These successes have also motivated the development of solar-to-CO_2RR systems based on PSCs. Furthermore, the easily tunable bandgap of perovskite solar cells has more significant potential for future application [29,30]. Recently, the combination of series-connected PSCs and CO_2RR demonstrated great potential, achieving over 6.3% of solar-to-CO_2RR efficiency. However, solar-to-CO_2RR efficiency still has opportunities to improve when the systems are utilized in solar cells with higher efficiency than the literature [10,31,32]. Furthermore, previous reports conducted solar-to-CO_2RR in one reactor without separation of each reaction. The reaction without separation brings about an increase of overpotential for the reaction due to the reaction environment. Moreover, an additional separation process of gas products is required without the separation of reactors.

Herein, we demonstrate the sustainable solar-to-CO_2RR system composed of electrodeposited Au dendrite electrode, Co-Pi electrode, and three series-connected PSCs as cathode, anode, and power source, respectively. To optimize the balance of proton supplement from water oxidation and CO_2RR rate, the catalytic activity of each electrode was measured with the 3-electrode system in a neutral electrolyte. Finally, we achieved 8% of solar-to-CO_2RR efficiency during the galvanostatic operation with separated reaction compartments by membrane for 12 h.

2. Results

To achieve the better catalytic activity of CO_2RR, we employed electrochemically deposited Au dendrite. To confirm the crystal structure of the electrodeposited Au dendrite, we performed an X-ray diffraction analysis for the deposited electrode (Figure S1). Face-centered cubic structure of Au peak was assigned at 2 θ = 38.5°, 44.7°, 64.7°, 77.6° corresponded to (111), (200), (220), and (311) indices, respectively (JCPDS # 04-0784) [33]. The morphology of Au dendrite was confirmed by taking field emission scanning electron microscopy (FE-SEM) images (Figure 1a). Nanocrystalline Au dendrite, which has 60–100 nm-sized dendrite branches, was deposited by an electrochemical deposition method.

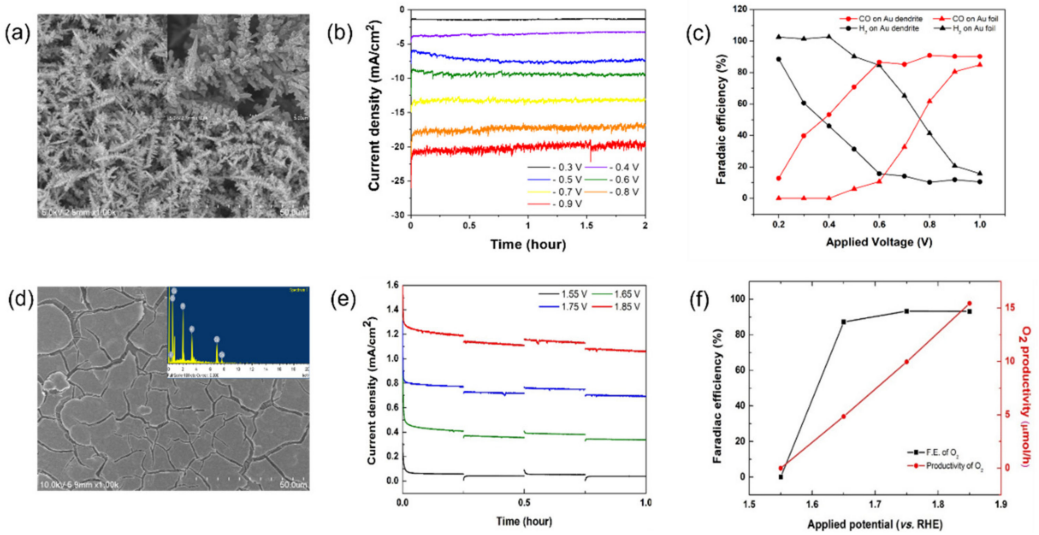

Figure 1. Electrochemical performances of cathode and anode: (**a**) SEM image of Au dendrite electrode. (**b**) Chronoamperometry test of CO_2 reduction by using Au dendrite electrode in the range from −0.3 V to −0.9 V (vs. RHE) in saturated 0.5 M $KHCO_3$ electrolyte. (**c**) Faradaic efficiency of Au dendrite and Au foil. (**d**) SEM image and EDS result of Co-Pi electrode. (**e**) Chronoamperometry test of water oxidation by using Co-Pi electrode in the range from 1.55 V to 1.85 V (vs. RHE) in KPi electrolyte. (**f**) Faradaic efficiency and productivity of O_2 on Co-Pi electrode.

To verify the catalytic stability for long-term electrochemical CO_2RR with Au electrode, Au dendrite, and foil electrode were tested for 2 h in 0.5M saturated $KHCO_3$ (pH ~7) in range of −0.2 to −0.9 V (vs. RHE) with a 3-electrode system [34]. As a result of chronoamperometry, the current density of Au dendrite was maintained for 2 h without any significant current density drop. Furthermore, current density was amplified than Au foil due to increased surface area. The maximum current density was measured 21 A/cm^2 at −0.9 V (vs. RHE), producing 112.76 μmol of CO. The productivity on Au dendrite shows at least 2-times higher than untreated Au foil in all potential ranges (Table S1). Enhanced productivity of CO on Au dendrite electrode than Au foil is due to the increased surface area, measured by roughness factor (Figure S2) [35]. Compared to the surface area of the unmodified Au foil, the surface area of Au dendrite was expanded 245 times. The value of surface area increase does not precisely correspond to the amount of productivity increase because the reaction is limited by adsorbed proton and CO_2 on the surface. However, we conclude that the surface area increase positively affects reaction productivity. To investigate the effect of nanostructured Au dendrite, we measured electrochemical impedance spectroscopy (EIS) of Au foil and dendrite (Figure S3, Table S2). EIS result revealed that ohmic and charge transfer resistance of Au dendrite was decreased than Au foil. This result indicated that facile electron transfer proceeded on Au dendrite. The facile electron transfers improved CO_2 reduction activity on Au dendrite, manifested in increasing current density [36].

Based on the chronoamperometry test and gas product analysis through in situ gas chromatography, we calculated the faradaic efficiency of Au dendrite and foil in the various applied potential region (Figure 1c). The details of reduction activity, including faradaic efficiency and productivity of H_2 and CO, are represented in Table S1. According to the result of faradaic efficiency, CO_2 reduction of Au dendrite was started from –0.2 V (vs. RHE) with 12.8% of CO conversion efficiency. The faradaic efficiency of CO by Au dendrite was increased as applied potential increased and exceeded over 85% after −0.6 V (vs. RHE). On the other hand, the efficiency of H_2 evolution was started with 88% at –0.2 V (vs. RHE) and gradually suppressed under 15% due to increasing CO productivity. Compared to the theoretical reduction potential from CO_2 to CO, which is –0.11 V (vs. RHE), this value indicates that Au dendrite successfully minimizes the CO_2/CO overpotential up to 0.09 V

(vs. RHE). In comparison, Au foil exhibits 0.39 V (vs. RHE) of overpotential for CO_2 reduction.

To establish the counterpart of the CO_2RR, we employed electrochemically deposited cobalt-phosphate (Co-Pi) thin film on FTO glass substrate, a well-known water oxidation catalyst working in a neutral medium such as potassium phosphate buffer (KPi, pH~7) [37]. It is crucial for CO_2RR that protons are sufficiently generated from water oxidation and then constantly diffused into the cathode through the Nafion membrane during the operation. For this reason, the Co-Pi catalyst, which oxidates water in the neutral medium, is the best candidate for the simultaneous reaction of CO_2RR and water oxidation known so far. To confirm the electrodeposited Co-Pi film, we analyzed the Co-Pi films by FE-SEM, electron energy-dispersive X-ray spectroscopy (EDS), and XRD showing that amorphous Co-Pi electrode was well deposited with 2.6 μm of thickness on FTO glass as previously reported [38] (Figure 1d and Figure S4). The electrodeposited Co-Pi electrode was tested for its water oxidation activity by using chronoamperometry for an hour. Figure 1e,f shows the catalytic activity of electrodeposited Co-Pi electrode in 0.1 M KPi buffer for an hour. The current density was maintained for an hour due to the self-healing property of the Co-Pi electrode. Overpotential for water oxidation on Co-Pi electrode shows relatively reduced value, which is 0.4 V (vs. RHE), and it corresponds to the previous report [38]. Also, the faradaic efficiency was reached over 90% after 1.65 V. The details of electrochemical results are summarized in Table S3.

For the electrochemical CO_2 reduction induced by sunlight, we confront several obstacles: (i) the electrochemical system should be conducted by galvanostatic method without reference electrode because solar cell generates DC photocurrent, (ii) CO_2 reduction and water oxidation proceed in the different electrolyte (i.e., CO_2 reduction in 0.5 M KHCO3 and water oxidation in 0.1 M KPi buffer), and (iii) during the electrochemical reaction, the proper amount of proton produced by water oxidation transfer to the cathode. For the application for simultaneous CO_2RR and water oxidation induced by solar energy system, we investigated the electrochemical catalytic activity by galvanostatic method (i.e., two-electrode system) with applied potential in the range from −2.2 to −2.9 V. Before the electrochemical test, the geometric size of each electrode should be adjusted for balancing a cathode and anode reaction rate.

Unlike the theoretical redox process, the reaction rate between CO_2RR on Au dendrite and water oxidation on the Co-Pi electrode is imbalanced in practical application. For this reason, we fixed the anode size for 6.25 cm^2 and optimized the reaction rate by varying cathode size. A prerequisite electrochemical test was conducted with two different geometric sizes of the cathode (i.e., Au S: 0.025 cm^2, Au L: 0.09 cm^2) for 2 h at the applied potential at −2.6 V. As we expected, the redox current was increased as increasing geometric size of Au electrode (Figure S5). In the case of the Au S electrode, the CO product selectivity for 2 h shows the outstanding result, which was 81.1% and 19.2% of faradaic efficiency for CO and H_2, respectively. However, despite increased redox current with Au L electrode, the selectivity toward conversion of CO has deteriorated to 27.1%, while the faradaic efficiency of H_2 was increased to 73.3% during the reaction process. To investigate the reason why the CO selectivity of the Au L electrode was diminished, we examined the productivity of CO. Figure 2a showed the chronological productivity of CO of each electrode. Comparing the productivity, CO production of Au L electrode was rapidly decreased after an hour.

On the other hand, CO production of Au S electrode was maintained an increasing tendency during the reaction. The productivity of CO from Au L and Au S electrodes was almost the same as 10.30 μmol/h and 9.54 μmol/h for 2 h. However, the hydrogen evolution rate (Figure 2b), which is a competitive reaction to CO_2RR, on the Au L electrode exhibits 47.51 μmol/h of H_2 while Au S electrode shows only 7.61 μmol/h. Based on the results, we postulate that the source of the massive amount of H_2 evolution on Au L electrode originated from proton dissolved in catholyte instead of a proton from water oxidation [39,40]. In other words, the amount of proton generation from the water oxidation is insufficient to process the efficient CO_2 reduction on the Au L electrode. To support

this postulation, we measured the pH of each electrolyte after the electrochemical reaction. Interestingly, the pH of the electrolyte from the Au L electrode was escalated from 7.1 to 8.3. In contrast, the pH of the electrolyte of the Au S electrode was maintained constantly. In addition, as the pH of the electrolyte increased, the solubility of the CO_2 decreased, resulting in a reducing CO productivity of the Au L electrode after 1 h of CO_2RR.

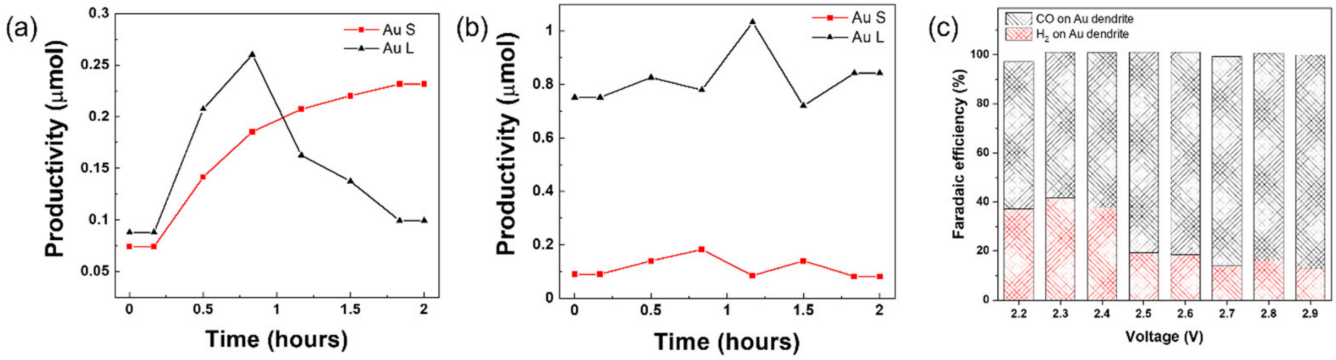

Figure 2. Galvanostatic test of CO_2 reduction and water oxidation. Productivity of (**a**) CO and (**b**) O_2 using Au S (red) and Au L (black) on the cathode. (**c**) Selectivity of CO and H_2 on Au S electrode in the range from 2.2 V to 2.9 V.

After balancing the reaction rate at each electrode, Au S electrode and Co-Pi electrode were conducted for CO_2 reduction and water oxidation in various applied potentials (i.e., −2.2 V to –2.9 V) for 4 h. As we mentioned earlier, the sum of overpotential of CO_2 reduction on Au dendrite and water oxidation on Co-Pi electrode in the three-electrode system was approximately 0.49 V. The reaction was supposed to start from 1.83 V (i.e., −0.11 V of theoretical CO_2 reduction potential +1.23 V of water oxidation potential +0.49 V of overpotential at each electrode). The voltage difference between the two values is originated from the ohmic loss, such as membrane and contact resistance between each electrode and electrolytes. Figure 2c and Figure S6 displayed the faradaic efficiency of CO_2 conversion reaction and chronological current versus applied potential, respectively. CO is started to produce from −2.2 V with 37.2% and 60.1% of faradaic efficiency toward CO and H_2, respectively, and increased their selectivity reached to over 85% after applied potential at −2.7 V. CO_2RR proceeded without a pH uprising, which means proton was successfully produced and diffused from anode to cathode.

Based on the galvanostatic results, we operate solar-driven CO_2RR and water oxidation. Electron generated from the solar cell and proton feedstock from water oxidation on Co-Pi electrode transfer to the cathode for CO_2RR. The electron generated from water oxidation fills in the hole in PSCs (Figure 3a). In this system, we employ three series-connected PSCs (geometric area: 0.282 cm^2) to generate good enough potential and current. Another critical factor for solar-to-CO_2RR stability is solar cell performance, such as proper voltage and current output and long-term light stability. The PSCs configuration used in this system was an n-i-p structure with FTO/b-TiO_2/mp-TiO_2/$(FAPbI_3)_{0.95}(MAPbBr_3)_{0.05}$/PTAA/Au. When we connected three PSCs, V_{max} and J_{max} values reached 2.88 V and 7.11 mA/cm^2 with 20.5% of power conversion efficiency (Figure 3b). To estimate the voltage and current density value of the solar-to-CO_2RR, we plotted the galvanostatic J–V curve based on the CO_2RR and water oxidation results. The galvanostatic J–V curve intersected at 2.68 V with 7.35 mA/cm^2 of the solar cell J–V curve. This result indicates that the power density of three series-connected PSCs is good enough to operate the reduction and oxidation reaction regardless overpotential of each reaction. Furthermore, the PSCs shows excellent long-term light stability for 12 h under ambient condition (25 °C/25% RH) with 1-sun LED light illumination. (Figure S7).

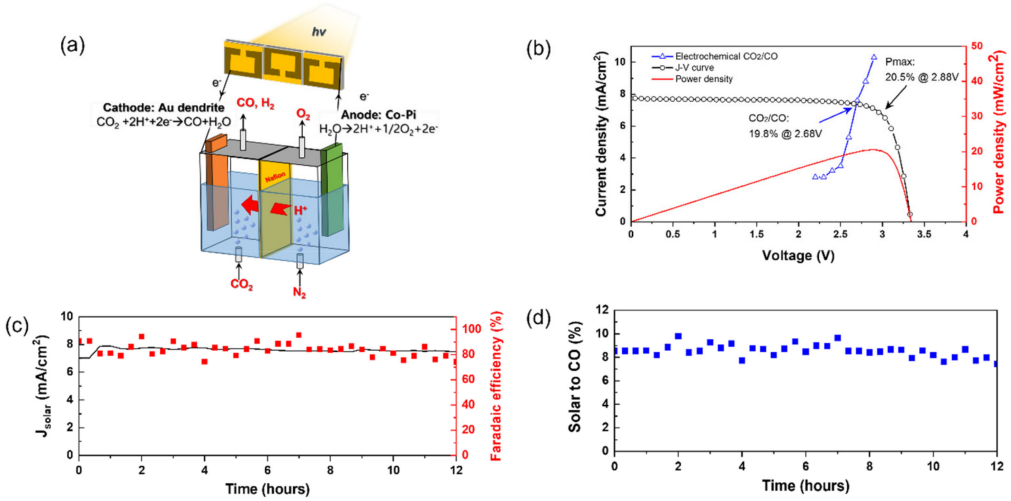

Figure 3. Performance of PV integrated CO_2 reduction system. (**a**) Schematic illustration of PV integrated CO_2 reduction and water oxidation system. (**b**) J–V curves of three series-connected perovskite cells under simulated AM 1.5G 1 Sun solar irradiation (black dots), overlaid with the matched J–V characteristic of the CO_2-reduction and water oxidation electrodes (blue dots). (**c**) Current density (black line), faradaic efficiency of CO (red dots), and (**d**) solar-to-CO conversion efficiency (blue dots) of the device during a 12-h stability test.

Through the solar-to-CO_2RR, we achieve over 80% of CO conversion faradaic efficiency for 12 h. The current density of the electrochemical reaction exhibited 7.1 mA/cm^2 and applied bias at each electrode was measured 2.7 V during the reaction (Figure 3c). These results correspond to the prediction as mentioned earlier based on the J–V galvanostatic curve, which intersected in 7.35 mA/cm^2 at 2.68V. Faradaic efficiency of solar-driven CO_2RR was also matched with galvanostatic results conducted without solar cell, which shows 85% of CO faradaic efficiency at 2.7 V of applied voltage. In addition, we attained solar to CO efficiency was measured over 8% without any significant drop during the reaction (Figure 3d). This value is higher than the previous report by M. Schreier et al., which showed 6.5% of solar to CO efficiency [10]. Furthermore, unlike processing in a single reactor, it can separate and collect CO and H_2 produced at the cathode and O_2 generated at the anode. Post-gas separation costs can be reduced when applied to the mass production system.

3. Conclusions

In conclusion, we employed electrodeposited Au dendrite and Co-Pi electrodes for CO_2RR and water oxidation catalyst. We adjusted reaction conditions such as the catalytic activity of CO_2 reduction and water oxidation, the optimum size of each electrode, and the reaction environment. CO_2RR was started at −0.2 V (vs. RHE) and reached over 80% of faradaic efficiency for CO conversion at −0.6 V (vs. RHE). Water oxidation with Co-Pi electrode was proceeded with 0.4 V of overpotential and attained over 80% of O_2 evolution efficiency. In the galvanostatic system, each reaction rate has been balanced by optimized geometric electrode size of Au dendrite and Co-Pi without pH change of electrolyte. Furthermore, the galvanostatic test provides insight into the selectivity of CO_2RR. It achieves over 80% from −2.7 V. Our solar-driven CO_2RR shows over 8% of solar-to-CO efficiency for 12 h without any significant drop. This system can be applied to total CO_2 conversion induced by solar energy, which is the ultimate solution for anthropogenic CO_2 problems and the development of alternative energy.

Supplementary Materials: The following are available online at https://www.mdpi.com/article/10.3390/en15010270/s1.

Author Contributions: J.C. carried out the electrochemical test and product analysis, N.J.J. carried out fabrication of PSC and stability test, N.J.J. and J.H.N. carried out the supervision of the project. All authors have read and agreed to the published version of the manuscript.

Funding: This research was supported by a grant from the Korea Research Institute of Chemical Technology (KRICT)(SS2122-20).

Conflicts of Interest: The authors declare no conflict of interest.

References

1. Marshall, J. Solar energy: Springtime for the artificial leaf. *Nature* **2014**, *510*, 22–24. [CrossRef] [PubMed]
2. Jang, Y.J.; Jeong, I.; Lee, J.; Lee, J.; Ko, M.J.; Lee, J.S. Unbiased sunlight-driven artificial photosynthesis of carbon monoxide from CO_2 using a ZnTe-based photocathode and a perovskite solar cell in tandem. *ACS Nano* **2016**, *10*, 6980–6987. [CrossRef] [PubMed]
3. Luo, J.; Im, J.-H.; Mayer Matthew, T.; Schreier, M.; Nazeeruddin Mohammad, K.; Park, N.-G.; Tilley, S.D.; Fan Hong, J.; Grätzel, M. Water photolysis at 12.3% efficiency via perovskite photovoltaics and earth-abundant catalysts. *Science* **2014**, *345*, 1593–1596. [CrossRef]
4. Gurudayal; Sabba, D.; Kumar, M.H.; Wong, L.H.; Barber, J.; Grätzel, M.; Mathews, N. Perovskite–hematite tandem cells for efficient overall solar driven water splitting. *Nano Lett.* **2015**, *15*, 3833–3839. [CrossRef]
5. Zhang, H.; Chen, Y.; Wang, H.; Wang, H.; Ma, W.; Zong, X.; Li, C. Carbon encapsulation of organic–inorganic hybrid perovskite toward efficient and stable photo-electrochemical carbon dioxide reduction. *Adv. Energy Mater.* **2020**, *10*, 2002105. [CrossRef]
6. Chen, J.; Dong, C.; Idriss, H.; Mohammed, O.F.; Bakr, O.M. Metal halide perovskites for solar-to-chemical fuel conversion. *Adv. Energy Mater.* **2020**, *10*, 1902433. [CrossRef]
7. Luo, J.; Vermaas, D.A.; Bi, D.; Hagfeldt, A.; Smith, W.A.; Grätzel, M. Bipolar membrane-assisted solar water splitting in optimal pH. *Adv. Energy Mater.* **2016**, *6*, 1600100. [CrossRef]
8. Chen, H.; Zhang, M.; Tran-Phu, T.; Bo, R.; Shi, L.; Di Bernardo, I.; Bing, J.; Pan, J.; Singh, S.; Lipton-Duffin, J.; et al. Integrating low-cost earth-abundant co-catalysts with encapsulated perovskite solar cells for efficient and stable overall solar water splitting. *Adv. Funct. Mater.* **2021**, *31*, 2008245. [CrossRef]
9. Koo, B.; Kim, D.; Boonmongkolras, P.; Pae, S.R.; Byun, S.; Kim, J.; Lee, J.H.; Kim, D.H.; Kim, S.; Ahn, B.T.; et al. Unassisted water splitting exceeding 9% solar-to-hydrogen conversion efficiency by Cu(In, Ga)$(S, Se)_2$ photocathode with modified surface band structure and halide perovskite solar cell. *ACS Appl. Energy Mater.* **2020**, *3*, 2296–2303. [CrossRef]
10. Schreier, M.; Curvat, L.; Giordano, F.; Steier, L.; Abate, A.; Zakeeruddin, S.M.; Luo, J.; Mayer, M.T.; Grätzel, M. Efficient photosynthesis of carbon monoxide from CO_2 using perovskite photovoltaics. *Nat. Commun.* **2015**, *6*, 7326. [CrossRef]
11. Mikkelsen, M.; Jørgensen, M.; Krebs, F.C. The teraton challenge. A review of fixation and transformation of carbon dioxide. *Energy Environ. Sci.* **2010**, *3*, 43–81. [CrossRef]
12. Schreier, M.; Gao, P.; Mayer, M.T.; Luo, J.; Moehl, T.; Nazeeruddin, M.K.; Tilley, S.D.; Grätzel, M. Efficient and selective carbon dioxide reduction on low cost protected Cu_2O photocathodes using a molecular catalyst. *Energy Environ. Sci.* **2015**, *8*, 855–861. [CrossRef]
13. Kang, P.; Chen, Z.; Nayak, A.; Zhang, S.; Meyer, T.J. Single catalyst electrocatalytic reduction of CO_2 in water to H^{2+}CO syngas mixtures with water oxidation to O_2. *Energy Environ. Sci.* **2014**, *7*, 4007–4012. [CrossRef]
14. Hori, Y. Electrochemical CO_2 Reduction on metal electrodes. In *Modern Aspects of Electrochemistry*; Vayenas, C.G., White, R.E., Gamboa-Aldeco, M.E., Eds.; Springer: New York, NY, USA, 2008; pp. 89–189.
15. Gattrell, M.; Gupta, N.; Co, A. A review of the aqueous electrochemical reduction of CO_2 to hydrocarbons at copper. *J. Electroanal. Chem.* **2006**, *594*, 1–19. [CrossRef]
16. Jiang, T.; Mowbray, D.J.; Dobrin, S.; Falsig, H.; Hvolbæk, B.; Bligaard, T.; Nørskov, J.K. Trends in CO oxidation rates for metal nanoparticles and close-packed, stepped, and kinked surfaces. *J. Phys. Chem. C* **2009**, *113*, 10548–10553. [CrossRef]
17. Falsig, H.; Hvolbaek, B.; Kristensen, I.S.; Jiang, T.; Bligaard, T.; Christensen, C.H.; Norskov, J.K. Trends in the catalytic CO oxidation activity of nanoparticles. *Angew. Chem. Int. Ed. Engl.* **2008**, *47*, 4835–4839. [CrossRef]
18. Gong, M.; Li, Y.; Wang, H.; Liang, Y.; Wu, J.Z.; Zhou, J.; Wang, J.; Regier, T.; Wei, F.; Dai, H. An advanced Ni-Fe layered double hydroxide electrocatalyst for water oxidation. *J. Am. Chem. Soc.* **2013**, *135*, 8452–8455. [CrossRef]
19. McDonald, K.J.; Choi, K.-S. Synthesis and photoelectrochemical properties of $Fe_2O_3/ZnFe_2O_4$ composite photoanodes for use in solar water oxidation. *Chem. Mater.* **2011**, *23*, 4863–4869. [CrossRef]
20. Masayuki Yagi, E.T.; Sakita, S.; Kuwabara, T.; Nagai, K. Self-Assembly of active IrO_2 colloid catalyst on an ITO electrode for efficient electrochemical water oxidation. *J. Phys. Chem. B* **2005**, *109*, 21489–21491. [CrossRef]
21. Lee, Y.; Suntivich, J.; May, K.J.; Perry, E.E.; Shao-Horn, Y. Synthesis and activities of rutile IrO_2 and RuO_2 nanoparticles for oxygen evolution in acid and alkaline solutions. *J. Phys. Chem. Lett.* **2012**, *3*, 399–404. [CrossRef] [PubMed]
22. Zeng, K.; Zhang, D. Recent progress in alkaline water electrolysis for hydrogen production and applications. *Prog. Energy Combust. Sci.* **2010**, *36*, 307–326. [CrossRef]
23. Jeon, N.J.; Noh, J.H.; Yang, W.S.; Kim, Y.C.; Ryu, S.; Seo, J.; Seok, S.I. Compositional engineering of perovskite materials for high-performance solar cells. *Nature* **2015**, *517*, 476–480. [CrossRef]

24. Yang Woon, S.; Noh Jun, H.; Jeon Nam, J.; Kim Young, C.; Ryu, S.; Seo, J.; Seok Sang, I. High-performance photovoltaic perovskite layers fabricated through intramolecular exchange. *Science* **2015**, *348*, 1234–1237. [CrossRef] [PubMed]
25. Jung, E.H.; Jeon, N.J.; Park, E.Y.; Moon, C.S.; Shin, T.J.; Yang, T.-Y.; Noh, J.H.; Seo, J. Efficient, stable and scalable perovskite solar cells using poly (3-hexylthiophene). *Nature* **2019**, *567*, 511–515. [CrossRef] [PubMed]
26. Min, H.; Lee, D.Y.; Kim, J.; Kim, G.; Lee, K.S.; Kim, J.; Paik, M.J.; Kim, Y.K.; Kim, K.S.; Kim, M.G.; et al. Perovskite solar cells with atomically coherent interlayers on SnO_2 electrodes. *Nature* **2021**, *598*, 444–450. [CrossRef] [PubMed]
27. Zhu, H.; Fu, Y.; Meng, F.; Wu, X.; Gong, Z.; Ding, Q.; Gustafsson, M.V.; Trinh, M.T.; Jin, S.; Zhu, X.Y. Lead halide perovskite nanowire lasers with low lasing thresholds and high quality factors. *Nat. Mater.* **2015**, *14*, 636–642. [CrossRef]
28. Luo, J.; Wang, X.; Li, S.; Liu, J.; Guo, Y.; Niu, G.; Yao, L.; Fu, Y.; Gao, L.; Dong, Q.; et al. Efficient and stable emission of warm-white light from lead-free halide double perovskites. *Nature* **2018**, *563*, 541–545. [CrossRef] [PubMed]
29. Kim, G.; Moon, C.S.; Yang, T.-Y.; Kim, Y.Y.; Chung, J.; Jung, E.H.; Shin, T.J.; Jeon, N.J.; Park, H.H.; Seo, J. A thermally induced perovskite crystal control strategy for efficient and photostable wide-bandgap perovskite solar cells. *Sol. RRL* **2020**, *4*, 2000033. [CrossRef]
30. Gharibzadeh, S.; Abdollahi Nejand, B.; Jakoby, M.; Abzieher, T.; Hauschild, D.; Moghadamzadeh, S.; Schwenzer, J.A.; Brenner, P.; Schmager, R.; Haghighirad, A.A.; et al. Record open-circuit voltage wide-bandgap perovskite solar cells utilizing 2D/3D perovskite heterostructure. *Adv. Energy Mater.* **2019**, *9*, 1803699. [CrossRef]
31. Huan, T.N.; Dalla Corte, D.A.; Lamaison, S.; Karapinar, D.; Lutz, L.; Menguy, N.; Foldyna, M.; Turren-Cruz, S.-H.; Hagfeldt, A.; Bella, F.; et al. Low-cost high-efficiency system for solar-driven conversion of CO_2 to hydrocarbons. *Proc. Natl. Acad. Sci. USA* **2019**, *116*, 9735. [CrossRef]
32. Chen, J.; Yin, J.; Zheng, X.; Ait Ahsaine, H.; Zhou, Y.; Dong, C.; Mohammed, O.F.; Takanabe, K.; Bakr, O.M. Compositionally screened eutectic catalytic coatings on halide perovskite photocathodes for photoassisted selective CO_2 reduction. *ACS Energy Lett.* **2019**, *4*, 1279–1286. [CrossRef]
33. Nesbitt, N.T.; Ma, M.; Trześniewski, B.J.; Jaszewski, S.; Tafti, F.; Burns, M.J.; Smith, W.A.; Naughton, M.J. Au dendrite electrocatalysts for CO_2 electrolysis. *J. Phys. Chem. C* **2018**, *122*, 10006–10016. [CrossRef]
34. Chen, Y.; Li, C.W.; Kanan, M.W. Aqueous CO_2 reduction at very low overpotential on oxide-derived Au nanoparticles. *J. Am. Chem. Soc.* **2012**, *134*, 19969–19972. [CrossRef]
35. Chung, J.; Won, D.H.; Koh, J.; Kim, E.-H.; Woo, S.I. Hierarchical Cu pillar electrodes for electrochemical CO_2 reduction to formic acid with low overpotential. *Phys. Chem. Chem. Phys.* **2016**, *18*, 6252–6258. [CrossRef] [PubMed]
36. Won da, H.; Choi, C.H.; Chung, J.; Chung, M.W.; Kim, E.H.; Woo, S.I. Rational design of a hierarchical tin dendrite electrode for efficient electrochemical reduction of CO_2. *ChemSusChem* **2015**, *8*, 3092–3098. [CrossRef]
37. Klahr, B.; Gimenez, S.; Fabregat-Santiago, F.; Bisquert, J.; Hamann, T.W. Photoelectrochemical and impedance spectroscopic investigation of water oxidation with "Co–Pi"-coated hematite electrodes. *J. Am. Chem. Soc.* **2012**, *134*, 16693–16700. [CrossRef]
38. Kanan, M.W.; Nocera, D.G. In situ formation of an oxygen-evolving catalyst in neutral water containing phosphate and Co^{2+}. *Science* **2008**, *321*, 1072–1075. [CrossRef]
39. Weekes, D.M.; Salvatore, D.A.; Reyes, A.; Huang, A.; Berlinguette, C.P. Electrolytic CO_2 reduction in a flow cell. *Acc. Chem. Res.* **2018**, *51*, 910–918. [CrossRef] [PubMed]
40. Endrődi, B.; Bencsik, G.; Darvas, F.; Jones, R.; Rajeshwar, K.; Janáky, C. Continuous-flow electroreduction of carbon dioxide. *Prog. Energy Combust. Sci.* **2017**, *62*, 133–154. [CrossRef]